JHEP HYPER VERSION

Received: *December 8, 1998,* Accepted: *March 23, 1999*

JHEP03(1999)017

On the disintegration of cosmic ray nuclei by solar photons

Luis N. Epele, Silvia Mollerach and Esteban Roulet

Depto. de Física, Universidad Nacional de La Plata
CC67, 1900, La Plata, Argentina
Email: epele@venus.fisica.unlp.edu.ar,
mollerach@venus.fisica.unlp.edu.ar, roulet@venus.fisica.unlp.edu.ar

Abstract: We discuss in detail the possibility of observing pairs of simultaneous parallel air showers produced by the fragments of cosmic ray nuclei which disintegrated in collisions with solar photons. We consider scenarios with different cosmic ray compositions, exploring the predicted rates for existing and planned detectors and looking for methods to extract information on the initial composition from the characteristics of the signal. In particular, we find that fluorescence detectors, such as HiRes or the Telescope Array, due to their low threshold ($\sim 10^{17}$ eV) and large area ($\sim 10^4$ km^2) may observe several events per year if cosmic rays at those energies are indeed heavy nuclei. The possibility of exploiting the angular orientation of the plane containing the two showers to further constrain the cosmic ray composition is also discussed.

Keywords: High Energy Cosmic Rays, Electromagnetic Processes and Properties.

Contents

1. Introduction

A long time ago, Zatsepin and Gerasimova [1, 2] suggested that the photo-disintegration of cosmic ray (CR) nuclei with solar photons could allow to study the CR composition at very high energies, $E \gtrsim 0.1$ EeV (1 EeV$= 10^{18}$ eV). Indeed, if a nucleon is stripped from a heavy nucleus on a photo-disintegration process, the comparison of the energies of the surviving nucleus with that of the emitted nucleon would directly provide the mass of the primary nucleus.

In order to be able to observe this kind of events, one needs that the probability for the disintegration process to take place as the nucleus traverses the solar system be non-negligible. It is also necessary that the separation among the fragments be sufficiently large so as to allow their individual identification but however not larger than the spatial coverage of the CR detectors.

To maximise the photo-disintegration probability, previous works have focused on CR energies for which the interaction with solar photons takes place at the giant resonance for photo-disintegration, i.e. such that the typical photon energy in the CR rest frame is 10–30 MeV (e.g. $E \simeq 1$ EeV for iron nuclei).

Regarding the separation among the fragments, Gerasimova and Zatsepin (GZ) originally estimated that it was of the order of 1 km [2], based on the splitting resulting from the transverse momenta acquired by the fragments in the disintegration process. However, as Zatsepin later realised, the dominant contribution to the splitting actually results from the deflection of the fragments in the solar system magnetic field (which was initially largely underestimated). This deflection depends on the charge to mass ratio of the fragments, and is hence different for nuclei, protons or neutrons.

In a recent reanalysis of this mechanism, Medina-Tanco and Watson [3] have performed detailed orbit integrations for incident Fe nuclei, using a realistic model for the solar system magnetic field. With these improved computations, they showed that the resulting separations are typically much larger than 10 km, and hence exceed the typical sizes of existing detectors, what strongly limits their observability. Going to higher energies in order to reduce the average shower separation down to an observable range has however the problem of a much reduced rate, since not only the cross section decreases outside the giant resonance, but more importantly the CR flux falls abruptly. Hence, the conclusion of that work regarding the observability of the effect was not encouraging.

In this work we want to extend previous analyses in several ways. Since the ultra-high energy CR are most probably not dominantly Fe nuclei, we study the GZ effect for different initial compositions. In order to cover all the range of possible CR nuclei masses we take as prototypical examples of heavy, intermediate and light compositions the nuclei ^{56}Fe, ^{16}O and ^{4}He. We find that although the cross sections are reduced going to lighter nuclei, for a given initial energy the separation among the fragments are smaller (approximately proportional to the mass number A), and hence this helps to make this kind of events observable. Also, since the energy of the emitted nucleon, which is smaller than the parent cosmic ray energy by a factor A, becomes higher the lighter is the initial mass composition, this allows for an easier detection of the nucleonic fragments.[1] We have also extended the cross sections beyond the pion-production threshold in this study.

The determination of the parent CR mass through the comparison of the energies of the two showers may be problematic in some cases. This occurs for instance if the determination of the nucleonic fragment energy is poor, as would happen if the energy is small so that only one detector in a ground array is hit by the shower (e.g. for a fragment energy $\simeq 10^{17}$ eV for Auger), or if more than one nucleon is emitted in the photo-disintegration. One may then attempt to use the size of the separation among the fragments to infer the initial composition. However, for a given initial energy the separation among the fragments also depends on the distance from the Earth at which the photo-disintegration took place. Hence, nuclei with different masses but interacting at different distances may give rise to equally separated showers. We have found that this degeneracy can be lifted in many cases by looking at the inclination of the plane containing the two fragments, since this angle depends on the distance from the Earth at which the photo-disintegration took place. Looking then at the whole available information (total energy, separation and inclination of the fragments) it will be possible to get further insights into the initial CR composition.

[1] For a Fe nucleus with $E \simeq 7\times10^{17}$ eV, as considered in [3], the emitted nucleon has $E \simeq 10^{16}$ eV, which is below the threshold of the large extended air shower arrays.

2. The photo-disintegration process

As a CR traverses the solar system, it encounters a flux of energetic ($\epsilon_\gamma \simeq 1$ eV) solar radiation. The lifetime for photo-disintegration off this radiation, computed in the rest frame of the CR nucleus (primed quantities), is just

$$\frac{1}{\tau'} = c \int_0^\infty \mathrm{d}\epsilon' \frac{\mathrm{d}n'}{\mathrm{d}\epsilon'} \sigma(\epsilon') \,, \tag{2.1}$$

with $\sigma(\epsilon')$ the photo-disintegration cross section. Transforming back to the lab (Earth) frame, using that $\epsilon' = \epsilon\gamma(1 + \beta\cos\alpha)$, where $\beta = v/c \simeq 1$ in terms of the CR velocity v, γ is the usual relativistic factor and α is the angle between the directions of propagation of the CR and of the photon, one finds for the CR mean free path

$$\frac{1}{\lambda(\xi)} = \int_0^\infty \mathrm{d}\epsilon \frac{\mathrm{d}n}{\mathrm{d}\epsilon}(\xi) \sigma(\epsilon')[1 + \beta\cos\alpha] \,. \tag{2.2}$$

Here ξ is a coordinate measuring the distance from the Earth along the arrival direction of the CR, so that if $\hat{\xi}$ is the unit vector in that direction, the CR velocity is $\mathbf{v} \simeq -c\hat{\xi}$ and $\cos\alpha = \hat{\xi} \cdot \hat{\mathbf{r}}$, with r the spherical radial coordinate centered in the sun.

The probability that an incoming CR suffers fragmentation along its path towards the Earth is then

$$\eta_{GZ} = 1 - \exp\left[- \int_0^\infty \mathrm{d}\xi \frac{1}{\lambda(\xi)} \right] . \tag{2.3}$$

This probability turns out to be small ($\ll 10^{-3}$), since $\lambda(\xi)$ is typically much larger than the characteristic solar system dimensions. For practical purposes, we will integrate up to $\xi_{max} = 5$ AU, since the contribution from larger distances turns out to be negligible due to the decreasing photon flux.

The solar photon flux can be obtained as a blackbody spectrum with the temperature of the solar surface, $T_s = 5770°\mathrm{K}$ ($k_B T_s \simeq 0.5$ eV), normalised so as to reproduce the solar luminosity, $L_\odot = 4\pi r^2 c \int \mathrm{d}\epsilon \; \epsilon \mathrm{d}n/\mathrm{d}\epsilon$. One then finds

$$\frac{\mathrm{d}n}{\mathrm{d}\epsilon} = 7.2 \times 10^7 \frac{\epsilon^2}{\exp(\epsilon/k_B T_s) - 1} \left(\frac{1 \text{ AU}}{r} \right)^2 [\text{eV cm}]^{-3} \,. \tag{2.4}$$

Regarding the photo-disintegration cross section σ, one can distinguish different regimes according to the photon energy in the nucleus rest frame. There is first the domain of the giant resonance, from the disintegration threshold ($\epsilon' \simeq 2$ MeV) up to ~ 30 MeV, in which a collective nuclear mode is excited with the subsequent emission of one (or possibly two) nucleons. Beyond the giant resonance and up to the pion production threshold ($\epsilon' \simeq 150$ MeV) the excited nucleus decays dominantly by two nucleon (quasi-deuteron effect) and multinucleon emission. Detailed fits to

the cross sections and branching fractions in these first two regimes were performed by Puget, Stecker and Bredekamp [4] in their study of the CR photo-disintegrations. For our purposes, it will be enough to adopt the simpler expressions for the total cross section given in [5], which are

$$\sigma(\epsilon') = \sigma_{GR}(\epsilon') \equiv 1.45A\frac{(\epsilon' T)^2}{(\epsilon'^2 - \epsilon_0^2)^2 + (\epsilon' T)^2}\text{mb} \qquad \text{for } \epsilon' < 30 \text{ MeV}, \tag{2.5}$$

where $T = 8$ MeV and $\epsilon_0 = 42.65A^{-0.21}$ MeV for $A > 4$ and $\epsilon_0 = 0.925A^{2.433}$ MeV for $A \leq 4$. For higher energies we take

$$\sigma(\epsilon') = \max\{\sigma_{GR}(\epsilon'), A/8 \text{ mb}\} \qquad \text{for } 30 \text{ MeV} < \epsilon' < 150 \text{ MeV}\,. \tag{2.6}$$

We do not cutoff σ_{GR} above 30 MeV since for light nuclei the peak of the giant resonance is already close to 30 MeV and the resonance is wide.

When considering light nuclei and/or very energetic CR ($E > 1$ EeV), it is necessary to consider in some detail the cross section above the pion production threshold. From this threshold up to $\epsilon' \simeq 600$ MeV, the disintegration is dominated by the delta production ($\gamma N \to \Delta \to N\pi$, where N is a nucleon).[2] In this regime, the cross section per nucleon is found to be almost independent of the target nucleus [6, 7]. Due to nuclear Fermi motion and interaction effects, the peak in this cross section is reduced and the resonance becomes somewhat wider than in the free proton case. (Higher resonances beyond $\Delta(1232)$ should also contribute for $\epsilon' \sim 1$ GeV.)

We have parametrised the total photo-absorption cross section in the region above the pion production threshold as

$$\sigma(\epsilon') = A\left[\frac{1}{8} + S\,\tilde{\epsilon}\,\exp\left(\frac{1-\tilde{\epsilon}^{\nu}}{\nu}\right)\right]\text{mb}\,, \qquad \text{for } \epsilon' > 150 \text{ MeV}\,, \tag{2.7}$$

where $\tilde{\epsilon} \equiv (\epsilon' - 150 \text{ MeV})/\epsilon_1$. A good fit to the experimental data [6] is obtained with $\epsilon_1 = 180$ MeV, $S = 0.3$ and $\nu = 1.8$, so that the maximum in the cross section ($\sigma_{max}/A = (1/8+S)$ mb$\simeq 0.4$ mb) occurs for an energy $\epsilon' = \epsilon_1 + 150$ MeV$\simeq 330$ MeV. The value of ν gives the right size of the resonance width.

Near the resonance peak, the one nucleon emission by direct knock-out is relevant, but the nucleon multiplicity increases at higher energies. The pions emitted will decay, for the typical γ factors considered ($\gamma \sim 10^7$–10^9), in a distance much shorter than 1 AU, and only their decay products can reach the atmosphere. However, these decay products will have an energy much below the initial CR energy and hence will pass largely unnoticed. Furthermore, the muons from $\pi^{\pm}$ decays will be significantly deflected by the solar system magnetic fields and hence arrive far from the nucleonic fragments.

[2] We note that using Rudstam type fits to the proton-nucleus cross section [8, 9] to estimate the photo-nuclear rates, or also photo-disintegration data from bremsstrahlung photons [10], one misses the strength of the Δ resonance peak.

3. The deflection of the fragments

After the parent CR photo-disintegrates, the fragments travel towards the Earth and are deflected by the solar system magnetic field with respect to their initial trajectories. The resulting deflection can be computed by integrating the transverse displacement due to the Lorentz force from the fragmentation point, at a distance ξ, up to the Earth.[3] In this way one finds

$$\mathbf{d}_f(\xi) = \frac{Z_f e}{A_f m\gamma c}\int_\xi^0 \mathrm{d}\xi' \int_{\xi'}^0 \mathrm{d}\xi'' \mathbf{B}(\xi'') \times \hat{\xi}\,, \tag{3.1}$$

where e and m are the proton charge and mass. The deflection d_f of each fragment is then proportional to its charge to mass ratio, Z_f/A_f. For the separation among the fragments what matters is the difference $|Z_1/A_1 - Z_2/A_2|$. If the emitted nucleon is a neutron, this is just $Z/(A-1)$, with Z and A associated to the charge and mass of the parent nucleus. If a proton is emitted, the difference is given by $(A-Z)/(A-1)$. Thus, the separation among the two fragments is approximately given by eq. (3.1) but replacing Z_f/A_f by 1/2 for Fe and O, and by 2/3 for He. In the case of multiple nucleon emission, all protons will be deflected by the same amount by the magnetic field (and all neutrons will be undeflected), so that they will produce essentially one shower (the typical separation of the strongly overlapped nucleonic showers, see footnote 3, is smaller than the separation of the detectors in the largest arrays, which is e.g. 1.5 km for Auger). The interesting possibility also appears of having three simultaneous showers caused by the main fragment, the emitted proton(s) and neutron(s), all contained in the same plane and equally separated.

As in [3], we consider for the solar system magnetic field the realistic model of Akasofu, Gray and Lee [11], which describes the field within the heliosphere, taken as a sphere of radius $r_2 = 20$ AU. It consists of four components (written here for an odd solar cycle, i.e. with the north polar region having the S magnetic pole):

a) The solar dipole contribution can be written, in cylindrical coordinates around the sun, as

$$B_z^{dip} = \frac{B_s r_1^3}{2}(\rho^2 - 2z^2)(z^2+\rho^2)^{-5/2}\,, \tag{3.2}$$

$$B_\rho^{dip} = -\frac{3B_s r_1^3}{2}\rho z (z^2+\rho^2)^{-5/2}\,, \tag{3.3}$$

$$B_\phi^{dip} = 0\,, \tag{3.4}$$

where $B_s r_1^3/2$ is the magnetic dipole moment of the sun. Taking r_1 to be the solar radius, $r_1 = R_\odot$, one has $B_s = 2$ Gauss.

[3] In the following we neglect the deflection due to the transverse momenta acquired by the nucleonic fragments in the photo-disintegration, since it leads to separations $\lesssim 0.2$ km $\sqrt{A/(E/\text{ EeV})}(\xi/1\text{ AU})$. The corresponding separation for an emitted alpha particle would be four times smaller.

b) The dynamo component arises from the rotation of the sun in the dipole field. It is generated by a sheet current distribution that flows outwards along the polar axis, then flows along the heliosphere towards the ecliptic plane and then radially inwards back to the sun. The resulting field is in the ϕ direction,

$$B_\phi^{dyn} = \mathrm{sign}(z) B_{\phi_0} \frac{\rho_0}{\rho}\,, \qquad r_1 < \sqrt{z^2+\rho^2} < r_2\,, \tag{3.5}$$

where $B_{\phi_0} = 3.5 \times 10^{-5}$ Gauss and $\rho_0 = 1$ AU.

c) The ring current component arises from a sheet equatorial current extending up to r_2, with current density $\propto \rho^{-2}$. The resulting magnetic field is given by

$$B_z^{ring} = {B_{\rho_0}\rho_0}^2 \int_0^\infty \mathrm{d}k\; kG(k) J_0(k\rho) \exp(-k|z|)\,, \tag{3.6}$$

$$B_\rho^{ring} = \mathrm{sign}(z) {B_{\rho_0}\rho_0}^2 \int_0^\infty \mathrm{d}k\; kG(k) J_1(k\rho) \exp(-k|z|)\,, \tag{3.7}$$

$$B_\phi^{ring} = 0\,, \tag{3.8}$$

where

$$G(k) = \frac{1}{k}\left[\sqrt{k^2+\frac{1}{r_2^2}} - \sqrt{k^2+\frac{1}{r_1^2}} + \frac{1}{r_1} - \frac{1}{r_2}\right],$$

$J_{0,1}$ are Bessel functions and $B_{\rho_0} = -3.5 \times 10^{-5}$ Gauss.

For the region of the solar system interesting for the present work ($r_1 \ll r < 5$ AU) the integrals in eqs. (3.6) and (3.7) can be approximated by taking the limit $r_1 \to 0$ and $r_2 \to \infty$ in $G(k)$. This gives

$$B_z^{ring} \simeq {B_{\rho_0}\rho_0}^2 |z| (z^2+\rho^2)^{-3/2}\,, \tag{3.9}$$

$$B_\rho^{ring} \simeq \mathrm{sign}(z) {B_{\rho_0}\rho_0}^2 \rho (z^2+\rho^2)^{-3/2}\,. \tag{3.10}$$

d) The sunspot component is approximated by an ensemble of 180 dipoles of radius 0.1 $R_\odot$ located in the equatorial plane, just below the solar surface at a radius of 0.8 $R_\odot$ (their expressions are similar to eq. (3.3) with $B_d = 1000$ Gauss). They provide a strong magnetic field near the sun surface and allow the ring current field lines to connect to the solar surface.

All the components change sign with the eleven years solar cycle. We plot in fig. 1 the three components of the magnetic field B_ϕ, B_ρ and B_z as a function of ρ for three different values of z. At large distances the dominant contribution is given by B_ϕ and B_ρ (due essentially to the dynamo and ring current components respectively).[4]

[4]The B_z component is at variance with the one plotted in ref. [3], and is proportional to r^{-3} for large radius. However, being this one the smallest componet, it has little impact on the results.

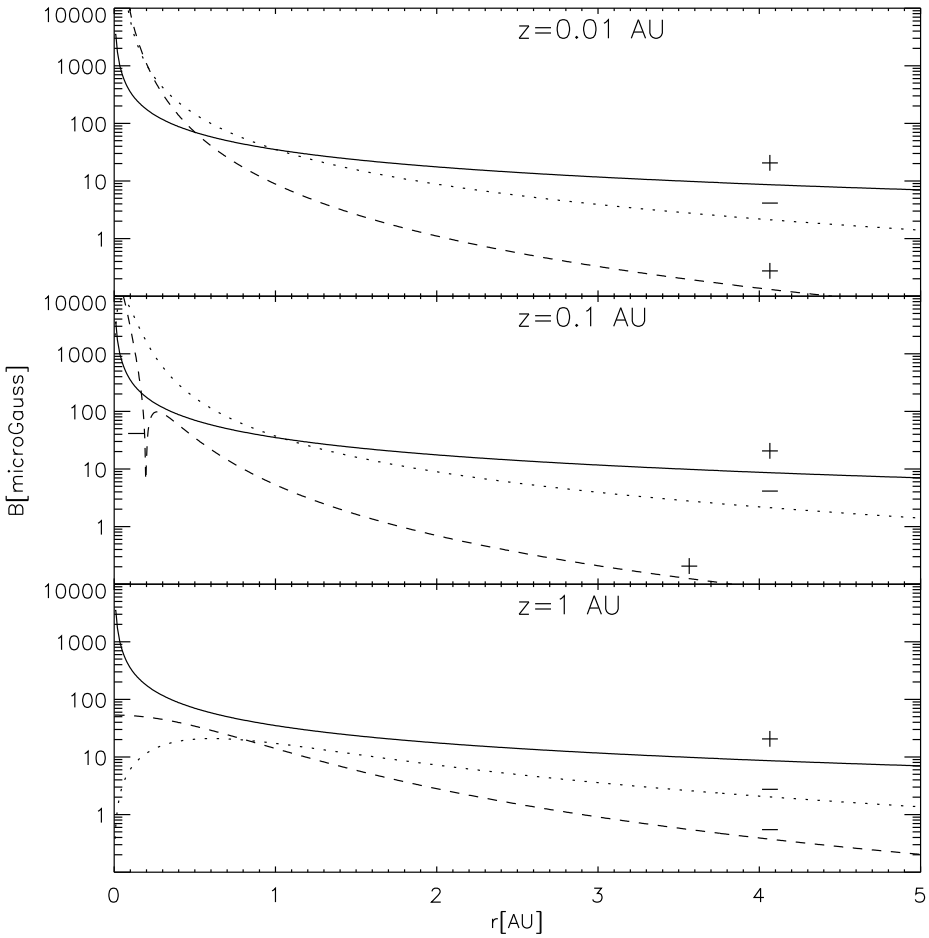

Figure 1: The three components of the solar system magnetic field, B_ϕ (solid line), B_ρ (dotted line) and B_z (dashed line), as a function of the radial cylindrical coordinate ρ for values of the z coordinate above the ecliptic $z = 0.01$ AU, 0.1 AU and 1 AU. We have plotted the modulus of each component and the sign is indicated in each curve.

We notice that the field model adopted gives a consistent description of Parker's spiral magnetic field configuration, and allows us to discuss the general features of the GZ events. Some departures from this simple model occur for instance due to the variation of the overall field normalization during the solar cycle or from a possible tilt of the magnetic equator with respect to the ecliptic, and these can be taken into account in the event of an actual detection. Sporadic magnetic perturbations such as shock waves produced by solar flares could also add some noise.

We describe the CR position by the distance ξ to the Earth and the latitude and longitude angular coordinates (b, ℓ), defined analogously to the Galactic ones, with $b = 0$ in the ecliptic plane and the sun at the origin of ℓ, with increasing ℓ values to the left (with the N up). The separation among the fragment positions can be decomposed along the b and ℓ directions, $\mathbf{d} = d_\ell \hat{\ell} + d_b \hat{b}$. We will use the modulus $d = \sqrt{d_\ell^2 + d_b^2}$ and the angle with respect to the $\hat{\ell}$ direction, $\mathrm{atan}(d_b/d_\ell)$, to describe it.

We can use the symmetry properties of the magnetic field about the ecliptic plane to infer the relationship among the separations between the fragments arriving from directions with the same longitude ℓ, but opposite latitude b, fragmenting at the same distance from the Earth (so that the sign of ξ_z changes, but the component of ξ in the ecliptic plane is the same). Under the reflection $z \to -z$, the radial and azimuthal components of $\mathbf{B}$ change sign, while B_z is invariant. Thus, the z component of the product $\mathbf{B} \times \hat{\xi}$ will change sign, while the orthogonal component remains unchanged. This means that $d_b(-b, \ell) = -d_b(b, \ell)$ and $d_\ell(-b, \ell) = d_\ell(b, \ell)$. Or, in other words, rays arriving from the same ℓ but opposite b and produced at the same distance from the Earth have separations between fragments equal in modulus but with opposite angles with respect to $\hat{\ell}$. Hence, when integrating the fragment orbits, only half of the celestial sphere needs to be evaluated.[5] We also note that in an even solar cycle all the field components are reversed, but this leaves unchanged both the separations and the angles.

4. Results

Typical separations for different parent nuclei are illustrated in fig. 2 for two different energies. The mean separation for each arrival direction is plotted (dashed lines), where the mean is weighted with the fragmentation probability for the photodisintegration processes to occur at different distances from the Earth, i.e.

$$\langle d(\ell, b) \rangle = \frac{1}{\eta_{GZ}} \int_0^{\xi_{max}} \mathrm{d}\xi d(\xi, \ell, b) \frac{\mathrm{d}\eta_{GZ}}{\mathrm{d}\xi} \,, \tag{4.1}$$

where $\mathrm{d}\eta_{GZ}/\mathrm{d}\xi \simeq 1/\lambda(\xi)$.

For Fe nuclei with $E = 1$ EeV most of the separations are larger than 100 km and are hence out of the reach of existing detectors, as noticed in ref. [3]. For lower energies this problem worsens, and for instance for $E = 0.1$ EeV most of the separations are larger than 500 km for Fe. The situation improves for lighter nuclei, due to the factor γ in eq. (3.1), which makes the separation approximately proportional to A for a fixed energy. For example, for He nuclei with $E = 1$ EeV most of the separations are smaller than 50 km, and hence within the range of existing or planned detectors.

The solid contours in fig. 2 correspond to the fragmentation probabilities η_{GZ} (and are labeled by $\eta_{GZ} \times 10^6$). Values of $\eta_{GZ} \sim 10^{-5}$–10^{-4} are obtained for Fe nuclei, while $\eta_{GZ} \sim 10^{-6}$–10^{-5} result for He and O.

In order to compute the rate of observation of these kind of events in a detector covering a surface S, one must only consider showers separated by distances smaller than $d_{max} \simeq \sqrt{S}$. The rates will be a convolution of the CR flux, the fragmentation

[5] This symmetry is not apparent in ref. [3], probably due to insufficient numerical accuracy.

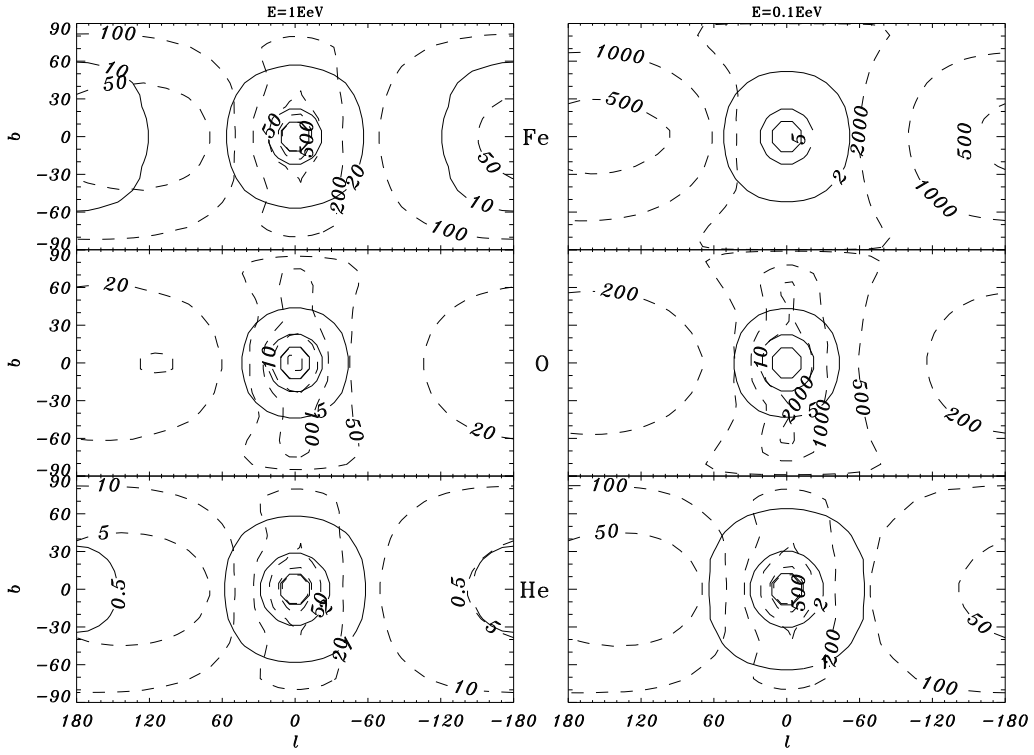

Figure 2: Mean fragments separation (dashed curves) and fragmentation probability (solid lines) contours for total energy $E = 0.1$ EeV and $E = 1$ EeV and for heavy (Fe), intermediate (O) and light (He) nuclei. The separation contours are labelled by their values in km units and the probabilities in units of 10^{-6}.

probability and the fraction of GZ events with $d < d_{max}$, $f_{d_{max}}(E)$. The areas (and thresholds) of the large extended air shower detectors we will consider are 100 km^2 for AGASA [12] ($E_{th} \simeq 1$ EeV), 3000 km^2 for Auger [13] ($E_{th} \simeq 1$ EeV), few$\times 10^4$ km^2 for HiRes [14] or the proposed Japanese Telescope Array [15] fluorescence detectors ($E_{th} \simeq 0.1$ EeV) and $\sim 10^6$ km^2 for the proposed OWL [16] type satellite fluorescence detectors ($E_{th} \simeq 10$ EeV).

Regarding the CR flux, above the knee in the spectrum ($E_{CR} > 3 \times 10^{15}$ eV), the measured flux is

$$\Phi(E_{CR} > E) \simeq 47 \left(\frac{\mathrm{EeV}}{E}\right)^2 [\mathrm{km}^2\ \mathrm{yr}\ \mathrm{sr}]^{-1}\,. \tag{4.2}$$

Due to the steepness of the spectrum ($\mathrm{d}\Phi/\mathrm{d}E \propto E^{-3}$), we will just estimate the rates of events from CR with energy above a given value E as

$$Rate(E_{CR} > E) \simeq \Phi(E_{CR} > E)\eta_{GZ}(E) f_{d_{max}}(E) S \epsilon_{dc} \Omega\,, \tag{4.3}$$

where fluorescence detectors have typical duty cycles $\epsilon_{dc} \simeq 0.1$ and Ω is the solid angle.

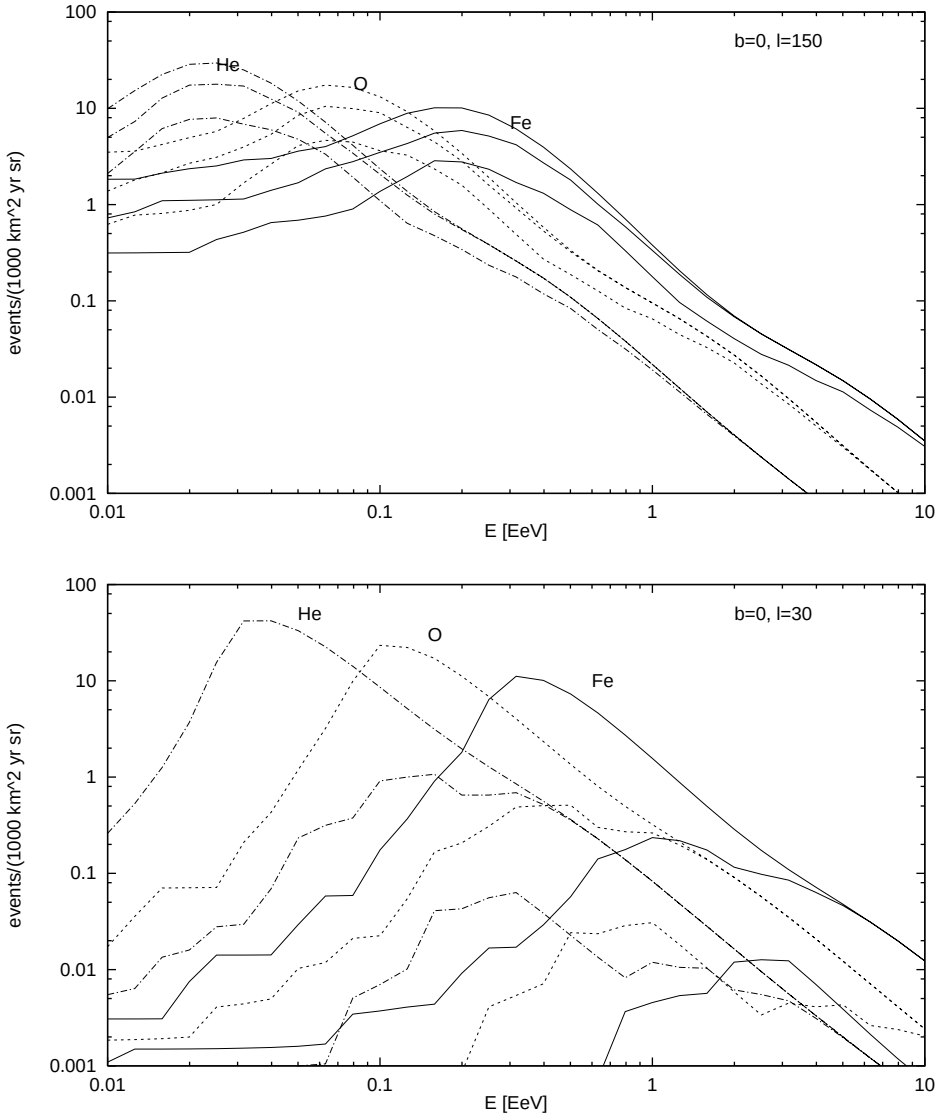

Figure 3: Expected rates of events per year and sr for a detector area of 1000 km^2 and for separation between fragments smaller than 1000 km (upper curves), 100 km (middle curves) and 10 km (lower curves). Solid lines correspond Fe, dashed lines to O and dot-dashed lines to He. Fig. 3a is for a night-time direction ($b = 0^\circ,\ \ell = 150^\circ$), while fig. 3$b$ for a direction close to the sun ($b = 0^\circ,\ \ell = 30^\circ$).

In fig. 3 we plot these rates as a function of the energy of the parent CR, for the three nuclei and for maximum distances of 1000, 100 and 10 km. Fig. 3a is for a night-time direction ($b = 0^\circ,\ \ell = 150^\circ$) while fig. 3$b$ is for a direction close to the sun ($b = 0^\circ,\ \ell = 30^\circ$).[6] It is clear that, if $d_{max} \lesssim 100$ km, the maximum rates per unit coverage are attained in the night side for energies $E \sim 10^{-2}$–1 EeV (depending on the nucleus considered) and exceed one event per year for coverages

[6]Note that in the day-side, $|\ell| < 90^\circ$, for increasing $|b|$ the average deflections decrease, enhancing the rates with respect to the $b = 0$ results of fig. 3. For the night-side the opposite will happen.

$S\ \Omega\ \epsilon_{dc} \gtrsim 10^3$ km^2 sr. Note that the AGASA array has an order of magnitude smaller coverage, while the Auger array, with $S \simeq 3000$ km^2 looks in this sense more promising. However, to be able to observe these events, low thresholds are required, and the emitted nucleon will not fire a tank in Auger if its energy is below 0.1 EeV. This means that to see both fragments, the parent CR should have an energy larger than $0.1A$ EeV, which for incident Fe nuclei is much larger than the typical threshold of the detector ($E_{th} \simeq 1$ EeV, corresponding to triggering with ~ 5 tanks). Hence, the rates for Auger are also quite small ($\lesssim 10^{-1}$events/yr). The most promising experiments for detecting these kind of events seem to be the large fluorescence detectors in construction (HiRes) or planned (Telescope Array), since besides having large areas ($\gtrsim\ 10^4$ km^2) they will have low thresholds (0.1 EeV). Furthermore, it is even possible that if the heavier fragment is above the threshold and triggers the detector, the lighter fragment is seen even if it has an energy somewhat below 0.1 EeV. With these arrays one will then expect few events per year for energies below 1 EeV if the CR are indeed not mainly protons. Larger detectors, as the proposed OWL and AIRWATCH satellites, have much higher thresholds, $E_{th}\ \simeq 10$EeV, and hence will have small rates ($\lesssim\ 0.3$ events/yr).

Considering the day side ($|\ell| < 90°$), only ground arrays can be employed, and looking at fig. 3*b* we see that the rates are very small for $d_{max} < 100$ km. This is due to the fact that most fragment separations are larger than the typical size of the detectors and become hence unobservable.

In the case of a positive detection of two simultaneous showers, if a single nucleon was emitted, the initial CR composition could be determined as $A \simeq\ (E_1 + E_2)/E_1$, with E_1 the energy of the less energetic shower and E_2 that of the most energetic one. This procedure will not lead to a precise determination of A if the nucleon shower energy is close to the threshold, and hence poorly determined, or if there was multiple nucleon emission, so that the smaller shower is actually produced by an unknown number of nucleons. There is however additional information about the CR composition, encoded in the separation between the detected fragments, which can be used to obtain a good determination of A also in these cases. From fig. 2 it is clear that, for a given initial energy and arrival direction, the average separations are quite sensitive to the CR composition. However, the distributions of separations are quite flat (see fig. 4) due to the wide range of distances from the Earth at which the photo-disintegration can occur (with the exception of the directions close to the sun, e.g. fig. 4*a*, for which the most likely location for the photo-disintegration interactions are for $\xi \simeq 1$ AU). This can result in different nuclei producing similar separations if they disintegrate at different distances.

We have found that this degeneracy can be lifted in many cases by looking at the inclination of the showers (i.e. at the angle $\mathrm{atan}(d_b/d_\ell)$). In fig. 5 we show the relations obtained between the separation d and the inclination angle, for $b = 10°$ (fig. 5*a*) and for $b = 45°$ (fig. 5*b*) and for different values of $\ell = 30°$, $60°$, $90°$, $120°$,

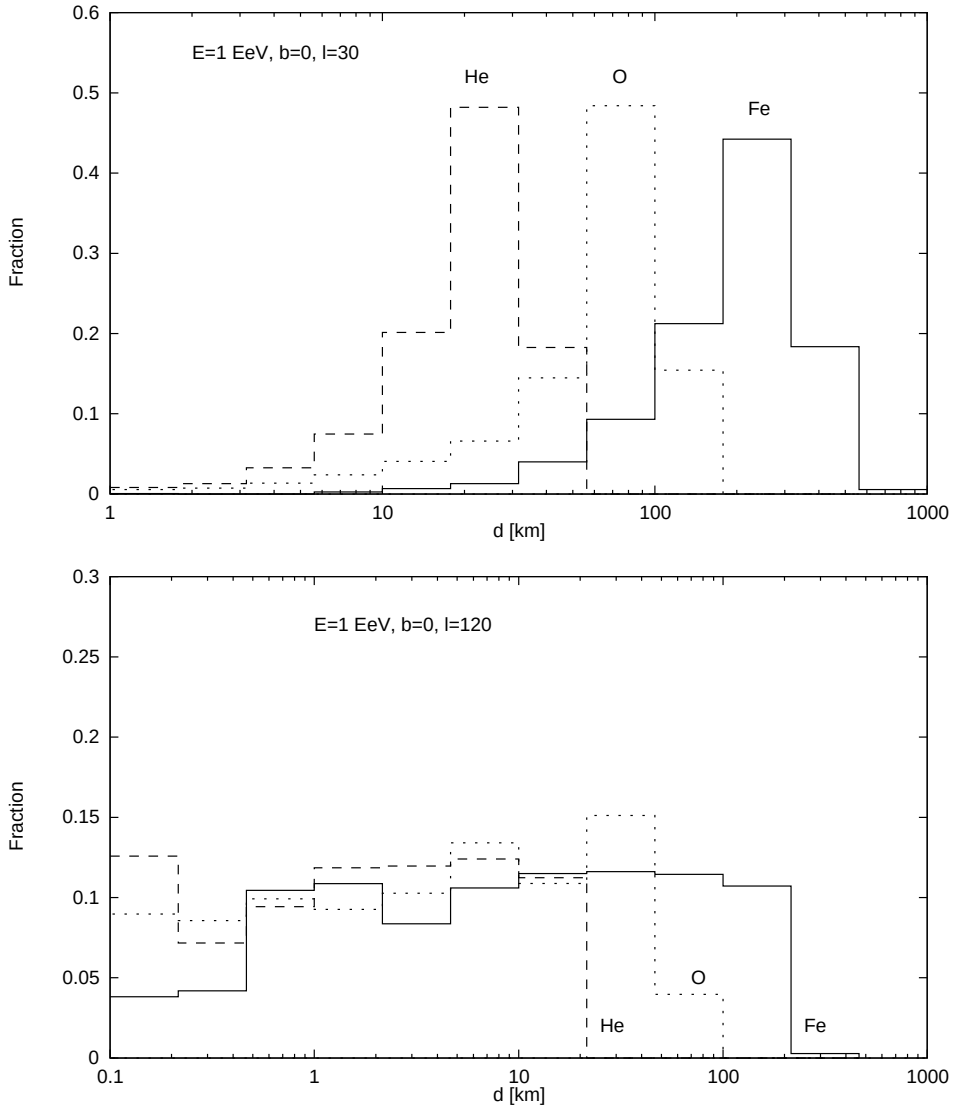

Figure 4: Distribution of the separation between fragments for a total energy of $E = 1$ EeV and for the three nuclei considered, Fe (solid line), O (dashed line) and He (dot-dashed line). Fig. 4*a* is for ($b = 0°,\ \ell = 30°$), while fig. 4*b* for ($b = 0°,\ \ell = 120°$). The histograms give the probability that the separation falls in the range of distances corresponding to each bin.

150°, 180°, 240° and 330°. One moves along the curves as the photo-disintegration distance ξ is varied. For the southern hemisphere ($b < 0°$), the inclination angle changes sign. Since the separations scale as $\gamma^{-1} \propto A/E$, what is plotted is $d \times (A/56) \times (\mathrm{EeV}/E)$.

Hence, knowing the total energy E, one may infer A by using plots like those in fig. 5. This is just done by plotting the d vs. angle curve for the arrival direction ($b,\ \ell$) of the observed CR. Confronting then this curve with the measured separation and inclination of the showers, and knowing the total energy E, A can be determined.

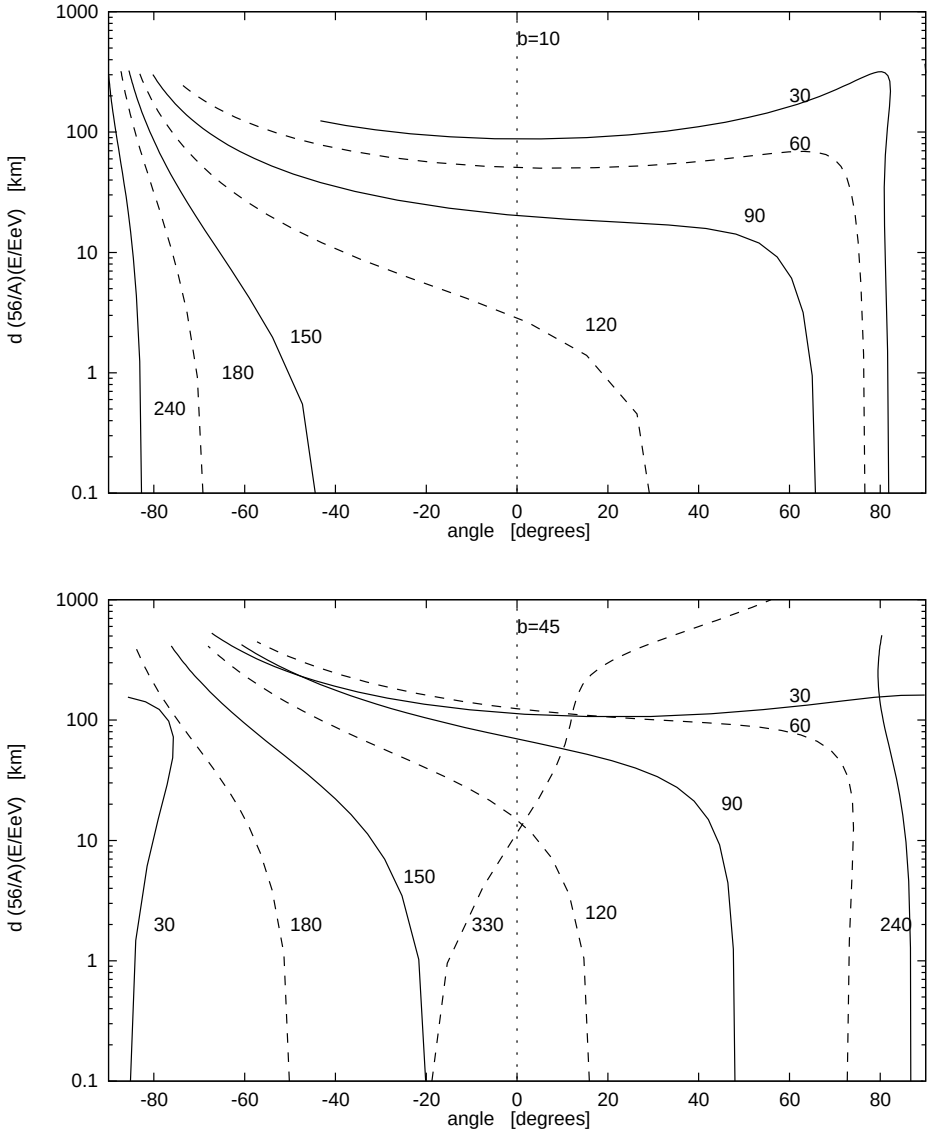

Figure 5: Separation vs. inclination angle of the fragments for arrival directions with $b = 10^\circ$ (fig. 5a) and $b = 45^\circ$ (fig. 5b), and for the ℓ values indicated in each line.

One can see that for many directions (e.g. $0^\circ < \ell < 180^\circ$ in fig. 5a) the inclination of the showers varies considerably as ξ is varied, and hence the inclination contains the information on the distance to the photo-disintegration point which allows the determination of A. In other directions (i.e. those leading to almost vertical curves) the resolving power of this method is instead not good.

In summary, we have explored in detail the possibility of detecting double shower events originating from the fragments produced in the photo-disintegration of a CR in a collision with a solar photon, for different compositions of the primary CR. The best possibilities are for the future large area fluorescence detectors, like HiRes and the Telescope Array, for which few events per year are expected if the CR of

energies larger than 0.1 EeV are indeed nuclei. These will be rare, peculiar events, but it would be interesting to detect them as they can give important information about the CR composition at ultra-high energies. The proposed method of using the separation and inclination of the showers to complement the analysis with the ratio of energies will also help to get a more precise determination of the composition of the parent CR.

Acknowledgments

Work partially supported by CONICET, Argentina.

References

[1] G.T. Zatsepin, *Dokl. Akad. Nauk. SSSR* **80** (1951) 577.

[2] N.M. Gerasimova and G.T. Zatsepin, *Sov. Phys. JETP* **11** (1960) 899.

[3] G.A. Medina-Tanco and A.A. Watson, `astro-ph/9808033`.

[4] J.L. Puget, F.W. Stecker and J.H. Bredekamp, *Astrophys. J.* **205** (1976) 638.

[5] S. Karakula and W. Tkaczyk, *Astropart. Phys.* **1** (1993) 229.

[6] J. Arends et al., *Phys. Lett.* **B 98** (1981) 423.

[7] J. Ahrens, *Nucl. Phys.* **A 446** (1985) 229c;
J. Ahrens and J. S. O'Connell, *Comments Nucl. Part. Phys.* **14** (1985) 245.

[8] R. Silberberg and C.H. Tsao, *Astrophys. J. Suppl. Series* **25** (1973) 315.

[9] J.W. Elbert and P. Sommers, *Astrophys. J.* **441** (1995) 151.

[10] G.G. Jonsson and K. Lindgren, *Phys. Scripta* **7** (1973) 49, ibidem **15** (1977) 308.

[11] S.I. Akasofu, P.C. Gray and L.C. Lee, *Planet. Space Sci.* **28** (1979) 609.

[12] See `http://www.icrr.u-tokyo.ac.jp/as/project/agasa.html`.

[13] See `http://www.auger.org`.

[14] See `http://bragg.physics.adelaide.edu.au/astrophysics/FlysEye.html`.

[15] See `http://www-ta.icrr.u-tokyo.ac.jp/`.

[16] See `http://lheawww.gsfc.nasa.gov/docs/gamcosray/hecr/OWL/`.